Intertwining topological order and broken symmetry
in a theory of fluctuating spin density waves

Shubhayu Chatterjee,[1] Subir Sachdev,[1,2] and Mathias S. Scheurer[1]

[1]*Department of Physics, Harvard University, Cambridge MA 02138, USA*
[2]*Perimeter Institute for Theoretical Physics, Waterloo, Ontario, Canada N2L 2Y5*
(Dated: September 29, 2017)

The pseudogap metal phase of the hole-doped cuprate superconductors has two seemingly unrelated characteristics: a gap in the electronic spectrum in the 'anti-nodal' region of the square lattice Brillouin zone, and discrete broken symmetries. We present a SU(2) gauge theory of quantum fluctuations of magnetically ordered states which appear in a classical theory of square lattice antiferromagnets, in a spin density wave mean field theory of the square lattice Hubbard model, and in a $\mathbb{CP}^1$ theory of spinons. This theory leads to metals with an antinodal gap, and topological order which intertwines with the observed broken symmetries.

A remarkable property of the pseudogap metal of the hole-doped cuprates is that it does not exhibit a 'large' Fermi surface of gapless electron-like quasiparticles excitations, *i.e.* the size of the Fermi surface is smaller than expected from the classic Luttinger theorem of Fermi liquid theory [1]. Instead it has a gap in the fermionic spectrum near the 'anti-nodal' points $((\pi, 0)$ and $(0, \pi))$ of the square lattice Brillouin zone. Gapless fermionic excitations appear to be present only along the diagonals of the Brillouin zone (the 'nodal' region). One way to obtain such a Fermi surface reconstruction is by a broken translational symmetry. However, there is no sign of broken translational symmetry over a wide intermediate temperature range [2], and also at low temperatures and intermediate doping [3], over which the pseudogap is present. With full translational symmetry, violations of the Luttinger theorem require the presence of topological order [4–6].

A seemingly unrelated property of the pseudogap metal is that it exhibits discrete broken symmetries, which preserve translations, over roughly the same region of the phase diagram over which there is an antinodal gap in the fermionic spectrum. The broken symmetries include lattice rotations, interpreted in terms of an Ising-nematic order [7–10], and one or both of inversion and time-reversal symmetry breaking [11–16]. Luttinger's theorem implies that none of these broken symmetries can induce the needed fermionic gap by themselves.

The co-existence of the antinodal gap and the broken symmetries can be explained by intertwining them [17–19], *i.e.* by exploiting flavors of topological order which are tied to specific broken symmetries. Here we show that broken lattice rotations, inversion, and time-reversal appear naturally in several models appropriate to the known cuprate electronic structure.

We consider quantum fluctuations of magnetically ordered states found in two different computations: a classical theory of frustrated, insulating antiferromagnets on the square lattice, and a spin density wave theory of

metallic states of the square lattice Hubbard model. The types of magnetically ordered states found are sketched in Fig. 1a. The quantum fluctuations of these states are described by a SU(2) gauge theory, and this leads to the loss of magnetic order, and the appearance of phases with topological order and an anti-nodal gap in the fermion spectrum. We find that the topological order intertwines with precisely the observed broken discrete symmetries, as shown in Fig. 1b. We further show that the same phases are also obtained naturally in a $\mathbb{CP}^1$ theory of bosonic spinons supplemented by Higgs fields conjugate to long-wavelength spinon pairs.

Magnetic order: We examine states in which the electron spin $\hat{\boldsymbol{S}}_i$ on site i of the square lattice, at position $\boldsymbol{r}_i$, has the expectation value

$$\left\langle \hat{\boldsymbol{S}}_i \right\rangle = N_0 \left[\cos\left(\boldsymbol{K} \cdot \boldsymbol{r}_i\right) \cos(\theta)\, \hat{\boldsymbol{e}}_x + \sin\left(\boldsymbol{K} \cdot \boldsymbol{r}_i\right) \cos(\theta)\, \hat{\boldsymbol{e}}_y \right.$$
$$\left. + \sin(\theta)\, \hat{\boldsymbol{e}}_z \right]. \tag{1}$$

The different states we find are (see Fig. 1a) (D′) a Néel state with collinear antiferromagnetism at wavevector (π, π), with $\boldsymbol{K} = (\pi, \pi)$, $\theta = 0$; (A′) a canted state, with (π, π) Néel order co-existing with a ferromagnet moment perpendicular to the Néel order, with $\boldsymbol{K} = (\pi, \pi)$, $0 < \theta < \pi/2$, (B′) a planar spiral state, in which the spins precess at an incommensurate wavevector $\boldsymbol{K}$ with $\theta = 0$; (C′) a conical spiral state, which is a planar spiral accompanied by a ferromagnetic moment perpendicular to the plane of the spiral [20] with $\boldsymbol{K}$ incommensurate, $0 < \theta < \pi/2$.

First, we study the square lattice spin Hamiltonian with near-neighbor antiferromagnetic exchange interactions $J_p > 0$, and ring exchange K [21–25]:

$$\mathcal{H}_J = \sum_{i<j} J_{ij}\, \hat{\boldsymbol{S}}_i \cdot \hat{\boldsymbol{S}}_j + 2K \sum_{\substack{k \quad \ell \\ j \square i}} \Big[(\hat{\boldsymbol{S}}_i \cdot \hat{\boldsymbol{S}}_j)(\hat{\boldsymbol{S}}_k \cdot \hat{\boldsymbol{S}}_\ell)$$
$$+ (\hat{\boldsymbol{S}}_i \cdot \hat{\boldsymbol{S}}_\ell)(\hat{\boldsymbol{S}}_k \cdot \hat{\boldsymbol{S}}_j) - (\hat{\boldsymbol{S}}_i \cdot \hat{\boldsymbol{S}}_k)(\hat{\boldsymbol{S}}_j \cdot \hat{\boldsymbol{S}}_\ell) \Big]. \tag{2}$$

$J_{ij} = J_p$ when i, j are p'th nearest neighbors, and we only allow J_p with $p = 1, 2, 3, 4$ non-zero. The classical
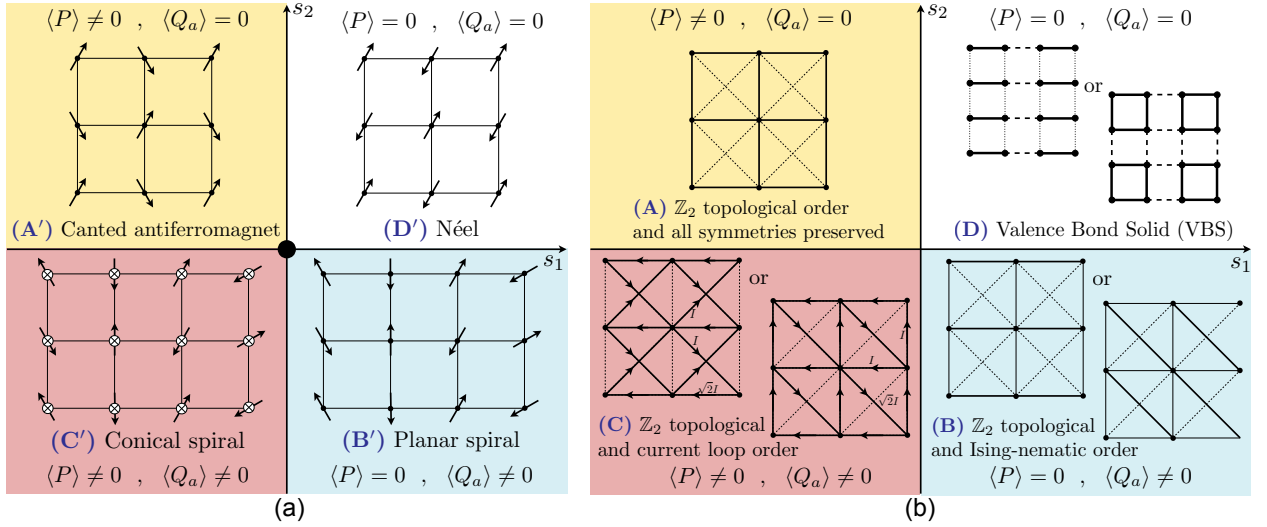
FIG. 1. (a) Schematics of the magnetically ordered states obtained in the classical antiferromagnet, and in the spin density wave theory of the Hubbard model. (b) Corresponding states obtained after quantum fluctuations restore spin rotation symmetry. Phase D has U(1) topological order in the metal, but is unstable to the appearance of VBS order in the insulator. The crossed circles in phase C′ indicate a canting of the spins into the plane. The labels s_1, s_2, P, Q_a refer to the $\mathbb{CP}^1$ theory: the phases in (a) are obtained for small g, and those in (b) for large g.

ground states are obtained by minimizing $\mathcal{H}_J$ over the set of states in Eq. (1); results are shown in Fig. 2a-c. We find the states A′, B′, C′, D′, all of which meet at a multicritical point, just as in the schematic phase diagram in Fig. 1a. A semiclassical theory of quantum fluctuations about these states, starting from the Néel state, appears in Appendix A.

For metallic states with spin density wave order, we study the Hubbard model

$$\mathcal{H}_U = -\sum_{i<j,\alpha} t_{ij} c_{i,\alpha}^\dagger c_{j,\alpha} - \mu \sum_{i,\alpha} c_{i,\alpha}^\dagger c_{i,\alpha} + U \sum_i \hat{n}_{i,\uparrow} \hat{n}_{i,\downarrow}$$

(3)

of electrons $c_{i,\alpha}$, with $\alpha = \uparrow, \downarrow$ a spin index, $t_{ij} = t_p$ when i, j are p'th nearest neighbors, and we take t_p with $p = 1, 2, 3, 4$ non-zero. U is the on-site Coulomb repulsion, and μ is the chemical potential. The electron density, $\hat{n}_{i,\alpha} \equiv c_{i,\alpha}^\dagger c_{i,\alpha}$, while the electron spin $\hat{S}_i \equiv (1/2) c_{i,\alpha}^\dagger \boldsymbol{\sigma}_{\alpha\beta} c_{i,\beta}$, with $\boldsymbol{\sigma}$ the Pauli matrices. We minimized $\mathcal{H}_U$ over the set of free fermion Slater determinant states obeying Eq. (1), while maintaining uniform charge and current densities; results are illustrated in Fig. 2d-f, and details appear in Appendix B. Again, note the appearance of the magnetic orders A′, B′, C′, D′, although now these co-exist with Fermi surfaces and metallic conduction.

SU(2) gauge theory: We describe quantum fluctuations about states of $\mathcal{H}_U$ obeying Eq. (1) by transforming the electrons to a rotating reference frame by a SU(2) matrix R_i [26]

$$\begin{pmatrix} c_{i,\uparrow} \\ c_{i,\downarrow} \end{pmatrix} = R_i \begin{pmatrix} \psi_{i,+} \\ \psi_{i,-} \end{pmatrix}, \qquad R_i^\dagger R_i = R_i R_i^\dagger = \mathbb{1}. \quad (4)$$

The fermions in the rotating reference frame are spinless 'chargons' ψ_s, with $s = \pm$, carrying the electromagnetic charge. In the same manner, the transformation of the electron spin operator $\hat{S}_i$ to the rotating reference frame is proportional to the 'Higgs' field H_i [26],

$$\boldsymbol{\sigma} \cdot \boldsymbol{H}_i \propto R_i^\dagger \boldsymbol{\sigma} \cdot \hat{\boldsymbol{S}}_i R_i. \quad (5)$$

The new variables, ψ, R, and H provide a formally redundant description of the physics of $\mathcal{H}_U$ as all observables are invariant under a SU(2) gauge transformation V_i under which

$$\begin{aligned} R_i &\to R_i V_i^\dagger \\ \boldsymbol{\sigma} \cdot \boldsymbol{H}_i &\to V_i \boldsymbol{\sigma} \cdot \boldsymbol{H}_i V_i^\dagger \end{aligned} \quad \begin{pmatrix} \psi_{i,+} \\ \psi_{i,-} \end{pmatrix} \to V_i \begin{pmatrix} \psi_{i,+} \\ \psi_{i,-} \end{pmatrix}, \quad (6)$$

while c_i and $\hat{S}_i$ are gauge invariant. The action of the SU(2) gauge transformation V_i, should be distinguished from the action of global SU(2) spin rotations Ω under which

$$\begin{aligned} R_i &\to \Omega R_i \\ \boldsymbol{\sigma} \cdot \hat{\boldsymbol{S}}_i &\to \Omega \boldsymbol{\sigma} \cdot \hat{\boldsymbol{S}}_i \Omega^\dagger \end{aligned} \quad \begin{pmatrix} c_{i\uparrow} \\ c_{i\downarrow} \end{pmatrix} \to \Omega \begin{pmatrix} c_{i\uparrow} \\ c_{i\downarrow} \end{pmatrix}, \quad (7)$$

while ψ and H are invariant.

In the language of this SU(2) gauge theory [26, 27], the phases with magnetic order obtained above appear when both R and H are condensed. We may choose a gauge in which $\langle R \rangle \propto \mathbb{1}$, and so the orientation of the H condensate is the same as that in Eq. (1),

$$\begin{aligned} \langle \boldsymbol{H}_i \rangle = H_0 \Big[&\cos\left(\boldsymbol{K} \cdot \boldsymbol{r}_i\right) \cos(\theta)\, \hat{\boldsymbol{e}}_x + \sin\left(\boldsymbol{K} \cdot \boldsymbol{r}_i\right) \cos(\theta)\, \hat{\boldsymbol{e}}_y \\ &+ \sin(\theta)\, \hat{\boldsymbol{e}}_z \Big]. \end{aligned} \quad (8)$$
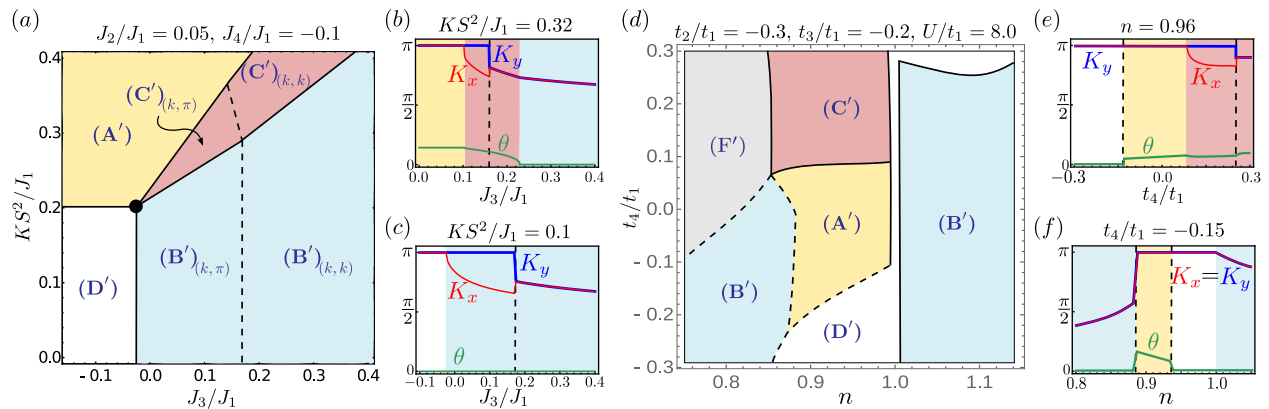
FIG. 2. (a) Phase diagram of $\mathcal{H}_J$, for a spin S model in the classical limit $S \to \infty$, exhibiting all phases of Fig. 1a. The subscript of the labels (B′) and (C′) indicates the wavevector $\boldsymbol{K} = (K_x, K_y)$ of the spiral. Note that the phases A′, C′, B′, D′ meet at a multicritical point, just as in Fig 1a. (b) and (c) show K_x, K_y, and the canting angle θ along two different one-dimensional cuts of the phase diagram in (a). The phase diagram resulting from the spin-density wave analysis of the Hubbard model (3) can be found in (d). Besides an additional ferromagnetic phase, denoted by (F′), we recover all the phases of the classical phase diagram in (a). Part (e) and (f) show one-dimensional cuts of the spin-density wave phase diagram. In all figures, solid (dashed) lines are used to represent second (first) order transitions.

We can now obtain the phases of $\mathcal{H}_U$ with quantum fluctuating spin density wave order, (A,B,C,D) shown in Fig. 1b, in a simple step: the quantum fluctuations lead to fluctuations in the orientation of the local magnetic order, and so remove the R condensate leading to $\langle R \rangle = 0$. The Higgs field $\boldsymbol{H}_i$ retains the condensate in Eq. (8) indicating that the magnitude of the local order is non-zero. In such a phase, spin rotation invariance is maintained with $\langle \hat{\boldsymbol{S}} \rangle = 0$, but the SU(2) gauge group has been 'Higgsed' down to a smaller gauge group which describes the topological order [17, 28–32]. The values of θ and $\boldsymbol{K}$ in phases (A,B,C,D) obey the same constraints as the corresponding magnetically ordered phases (A′, B′, C′, D′). In phase D, the gauge group is broken down to U(1), and there is a potentially gapless emergent 'photon'; in an insulator, monopole condensation drives confinement and the appearance of VBS order, but the photon survives in a metallic, U(1) 'algebraic charge liquid' (ACL) state [33] (which is eventually unstable to fermion pairing and superconductivity [34]). The remaining phases A,B,C have a non-collinear configuration of $\langle \boldsymbol{H}_i \rangle$ and then only $\mathbb{Z}_2$ topological order survives [17]: such states are ACLs with stable, gapped, 'vison' excitations carrying $\mathbb{Z}_2$ gauge flux which cannot be created singly by any local operator. Phase A breaks no symmetries, phase B breaks lattice rotation symmetry leading to Ising-nematic order [17, 28], and phase C has broken time-reversal and mirror symmetries (but not their product), leading to current loop order [35]. All the 4 ACL phases (A,B,C,D) may also become 'fractionalized Fermi liquids' (FL*) [4, 5] by formation of bound states between the chargons and R; the FL* states have a Pauli contribution to the spin susceptibility from the reconstructed Fermi surfaces.

The structure of the fermionic excitations in the phases of Fig. 1b, and the possible broken symmetries in the

$\mathbb{Z}_2$ phases, can be understood from an effective Hamiltonian for the chargons. As described in Appendix C, a Hubbard-Stratonovich transformation on $\mathcal{H}_U$, followed by the change of variables in Eqs. (4) and (5), and a mean field decoupling leads to

$$\mathcal{H}_\psi = -\sum_{i<j,s} t_{ij} Z_{ij} \psi_{i,s}^\dagger \psi_{j,s} - \mu \sum_{i,s} \psi_{i,s}^\dagger \psi_{i,s} - \sum_{i,s,s'} \boldsymbol{H}_i \cdot \psi_{i,s}^\dagger \boldsymbol{\sigma}_{ss'} \psi_{i,s'} . \tag{9}$$

The chargons inherit their hopping from the electrons, apart from a renormalization factor Z_{ij}, and experience a Zeeman-like coupling to a local field given by the condensate of $\boldsymbol{H}$: so the Fermi surface of ψ reconstructs in the same manner as the Fermi surface of c in the phases with conventional spin density wave order. Note that this happens here even though translational symmetry is fully preserved in all gauge-invariant observables; the apparent breaking of translational symmetry in the Higgs condensate in Eq. (8) does not transfer to any gauge invariant observables, showing how the Luttinger theorem can be violated by the topological order [4–6] in Higgs phases. However, other symmetries are broken in gauge-invariant observables: Appendix C examines bond and current variables, which are bilinears in ψ, and finds that they break symmetries in the phases B and C noted above.

$\mathbb{CP}^1$ **theory:** We now present an alternative description of all 8 phases in Fig. 1 starting from the popular $\mathbb{CP}^1$ theory of quantum antiferromagnets. In principle (as we note below, and in Appendix D, this theory can be derived from the SU(2) gauge theory above after integrating out the fermionic chargons, and representing R in terms

of a bosonic spinon field z_α by

$$R_i = \begin{pmatrix} z_{i,\uparrow} & -z_{i,\downarrow}^* \\ z_{i,\downarrow} & z_{i,\uparrow}^* \end{pmatrix}, \qquad |z_{i,\uparrow}|^2 + |z_{i,\downarrow}|^2 = 1. \qquad (10)$$

However, integrating out the chargons is only safe when there is a chargon gap, and so the theories below can compute critical properties of phase transitions only in insulators.

We will not start here from the SU(2) gauge theory, but present a direct derivation from earlier analyses of the quantum fluctuations of a $S = 1/2$ square lattice antiferromagnet near a Néel state, which obtained the following action [36] for a $\mathbb{CP}^1$ theory over two-dimensional space ($r = (x, y)$) and time (t)

$$\mathcal{S} = \frac{1}{g} \int d^2 r dt \, |(\partial_\mu - i a_\mu) z_\alpha|^2 + \mathcal{S}_B. \qquad (11)$$

Here μ runs over 3 spacetime components, and a_μ is an emergent U(1) gauge field. The local Néel order $\boldsymbol{n}$ is related to the z_α by $\boldsymbol{n} = z_\alpha^* \boldsymbol{\sigma}_{\alpha\beta} z_\beta$ where $\boldsymbol{\sigma}$ are the Pauli matrices. The U(1) gauge flux is defined modulo 2π, and so the gauge field is compact and monopole configurations with total flux 2π are permitted in the path integral. The continuum action in Eq. (11) should be regularized to allow such monopoles. $\mathcal{S}_B$ is the Berry phase of the monopoles [37–39]. Monopoles are suppressed in the states with $\mathbb{Z}_2$ topological order [17, 28], and so we do not display the explicit form of $\mathcal{S}_B$.

The phases of the $\mathbb{CP}^1$ theory in Eq. (11) have been extensively studied. For small g, we have the conventional Néel state, D′ in Fig. 1a, with $\langle z_\alpha \rangle \neq 0$ and $\langle \boldsymbol{n} \rangle \neq 0$. For large g, the z_α are gapped, and the confinement in the compact U(1) gauge theory leads to valence bond solid (VBS) order [38, 39], which is phase D in Fig. 1b. A deconfined critical theory describes the transition between these phases [40].

We now want to extend the theory in Eq. (11) to avoid confinement and obtain states with topological order. In a compact U(1) gauge theory, condensing a Higgs field with charge 2 leads to a phase with deconfined $\mathbb{Z}_2$ charges [41]. Such a deconfined phase has the $\mathbb{Z}_2$ topological order [17, 28–32] of interest to us here. So we search for candidate Higgs fields with charge 2, composed of pairs of long-wavelength spinons, z_α. We also require the Higgs field to be spin rotation invariant, because we want the $\mathbb{Z}_2$ topological order to persist in phases without magnetic order. The simplest candidate without spacetime gradients, $\varepsilon_{\alpha\beta} z_\alpha z_\beta$ (where $\varepsilon_{\alpha\beta}$ is the unit antisymmetric tensor) vanishes identically. Therefore, we are led to the following Higgs candidates with a single gradient ($a = x, y$)

$$P \sim \varepsilon_{\alpha\beta} z_\alpha \partial_t z_\beta \quad , \quad Q_a \sim \varepsilon_{\alpha\beta} z_\alpha \partial_a z_\beta \,. \qquad (12)$$

These Higgs fields have been considered separately before. Condensing Q_a was the route to $\mathbb{Z}_2$ topological order in Ref. 28, while P appeared more recently in Ref. 42.

	$\mathcal{T}$	T_x	I_x	$R_{\pi/2}$
z_α	$\varepsilon_{\alpha\beta} z_\beta$	$\varepsilon_{\alpha\beta} z_\beta^*$	z_α	z_α
Q_x	Q_x	Q_x^*	$-Q_x$	Q_y
Q_y	Q_y	Q_y^*	Q_y	$-Q_x$
P	$-P$	P^*	P	P

TABLE I. Symmetry signatures of various fields under time reversal ($\mathcal{T}$), translation by a lattice spacing along x (T_x), reflection about a lattice site with $x \to -x$, $y \to y$ (I_x), and rotation by $\pi/2$ about a lattice site with $x \to y$, $y \to -x$ ($R_{\pi/2}$).

The effective action for these Higgs fields, and the properties of the Higgs phases, follow straightforwardly from their transformations under the square lattice space group and time-reversal: we collect these in Table I. From these transformations, we can add to the action $\mathcal{S} \to \mathcal{S} + \int d^2 r dt \, \mathcal{L}_{P,Q}$

$$\begin{aligned} \mathcal{L}_{P,Q} = & \, |(\partial_\mu - 2 i a_\mu) P|^2 + |(\partial_\mu - 2 i a_\mu) Q_a|^2 \qquad (13) \\ & + \lambda_1 P^* \varepsilon_{\alpha\beta} z_\alpha \partial_t z_\beta + \lambda_2 Q_a^* \varepsilon_{\alpha\beta} z_\alpha \partial_a z_\beta + \text{H.c.} \\ & - s_1 |P|^2 - s_2 |Q_a|^2 - u_1 |P|^4 - u_2 |Q_a|^4, + \dots \end{aligned}$$

where we do not display other quartic and higher order terms in the Higgs potential.

For large g, we have $\langle z_\alpha \rangle = 0$, and can then determine the spin liquid phases by minimizing the Higgs potential as a function of s_1 and s_2. When there is no Higgs condensate, we noted earlier that we obtain phase D in Fig. 1b. Fig. 1b also indicates that the phases A,B,C are obtained when one or both of the P and Q_a condensates are present. This is justified in Appendix D by a computation of the quadratic effective action for the z_α from the SU(2) gauge theory: we find just the terms with linear temporal and/or spatial derivatives as would be expected from the presence of P and/or Q_a condensates in $\mathcal{L}_{P,Q}$.

We can confirm this identification from the symmetry transformations in Table I:
(A) There is only a P condensate, and the gauge-invariant quantity $|P|^2$ is invariant under all symmetry operations. Consequently this is a $\mathbb{Z}_2$ spin liquid with no broken symmetries; it has been previously studied by Yang and Wang [42] using bosonic spinons.
(B) With a Q_a condensate, one of the two gauge-invariant quantities $|Q_x|^2 - |Q_y|^2$ or $Q_x^* Q_y + Q_x Q_y^*$ must have a non-zero expectation value. Table I shows that these imply Ising-nematic order, as described previously [17, 28, 43]. We also require $\langle Q_x \rangle \langle Q_y^* \rangle$ to be real to avoid breaking translational symmetry.
(C) With both and P and Q_a condensates non-zero we can define the gauge invariant order parameter $O_a = P Q_a^* + P^* Q_a$ (again $\langle P \rangle \langle Q_a^* \rangle$ should be real to avoid translational symmetry breaking). The symmetry transformations of O_a show that it is precisely the 'current-loop' order parameter of Ref. 19: it is odd under reflection and time-reversal but not their product.

A similar analysis can be carried out at small g, where

z_α condenses and breaks spin rotation symmetry. The structure of the condensate is determined by the eignmodes of the z_α dispersion in the A,B,C,D phases, and this determines that the corresponding magnetically ordered states are precisely A′,B′,C′,D′, as in Fig. 1a.

We have shown here that a class of topological orders intertwine with the observed broken discrete symmetries in the pseudogap phase of the hole doped cuprates. The same topological orders emerge from a theory of quantum fluctuations of magnetically ordered states obtained by four different methods: the frustrated classical antiferromagnet, the semiclassical non-linear sigma model, the spin density wave theory, and the $\mathbb{CP}^1$ theory supplemented by the Higgs fields obtained by pairing spinons at long wavelengths. The intertwining of topological or-

der and symmetries can explain why the symmetries are restored when the pseudogap in the fermion spectrum disappears at large doping.

Appendix A: O(3) non-linear sigma model

We examined a semi-classical O(3) non-linear sigma model of quantum fluctuations of $\mathcal{H}_J$, which expresses $\hat{\boldsymbol{S}}_i$ in terms of the Néel field $\boldsymbol{n}(r,t)$ and the canonically conjugate uniform magnetization density $\boldsymbol{L}(r,t)$

$$\hat{\boldsymbol{S}}_i = S\eta_i \boldsymbol{n}_i \sqrt{1 - \boldsymbol{L}_i^2/S^2} + \boldsymbol{L}_i \tag{A1}$$

$$\boldsymbol{n}^2 = 1 \quad , \quad \boldsymbol{n} \cdot \boldsymbol{L} = 0, \tag{A2}$$

where $\eta_i = \pm 1$ on the two sublattices, $\boldsymbol{n}_i \equiv \boldsymbol{n}(r_i, t)$ and similarly for $\boldsymbol{L}_i$. Inserting Eq. (A1) into Eq. (2), and performing an expansion to fourth order in spatial gradients and powers of $\boldsymbol{L}$, we obtain $\mathcal{H}_J = \int d^2 r\, \overline{\mathcal{H}}_J$ (the lattice spacing has been set to unity):

$$
\begin{aligned}
\overline{\mathcal{H}}_J =\ & \frac{S^2(J_1 - 2J_2 - 4J_3 + 10J_4)}{2} \left[(\partial_x \boldsymbol{n})^2 + (\partial_y \boldsymbol{n})^2 \right] \\
& + 4(J_1 + 2J_4 - 4KS^2)\boldsymbol{L}^2 \\
& - \frac{(J_1 - 2J_2 - 4J_3 + 10J_4 - 8KS^2)}{2} \boldsymbol{L}^2 \left[(\partial_x \boldsymbol{n})^2 + (\partial_y \boldsymbol{n})^2 \right] \\
& - \frac{S^2(J_1 - 2J_2 - 16J_3 + 34J_4)}{24} \left[(\partial_x^2 \boldsymbol{n})^2 + (\partial_y^2 \boldsymbol{n})^2 \right] \\
& - \frac{(J_1 + 2J_2 + 4J_3 + 10J_4 - 8KS^2)}{2} \left[(\partial_x \boldsymbol{L})^2 + (\partial_y \boldsymbol{L})^2 \right] \\
& + \frac{S^2(J_2 - 8J_4 - 2KS^2)}{2} (\partial_x^2 \boldsymbol{n}) \cdot (\partial_y^2 \boldsymbol{n}) \\
& - 8KS^2 \left[(\boldsymbol{L} \cdot \partial_x \boldsymbol{n})^2 + (\boldsymbol{L} \cdot \partial_y \boldsymbol{n})^2 \right] \\
& - KS^4 [(\partial_x \boldsymbol{n}).(\partial_x \boldsymbol{n})][(\partial_y \boldsymbol{n}).(\partial_y \boldsymbol{n})] \\
& + 2KS^4 [(\partial_x \boldsymbol{n}).(\partial_y \boldsymbol{n})]^2 + 16K[\boldsymbol{L}^2]^2 \,.
\end{aligned}
\tag{A3}
$$

It is useful to extract the terms important for identifying the phases

$$\overline{\mathcal{H}}_J = \frac{\rho_s}{2}(\partial_a \boldsymbol{n})^2 + \frac{1}{2\chi_\perp}\boldsymbol{L}^2 + C_1(\boldsymbol{L}^2)^2 + C_2(\partial_a \boldsymbol{L})^2 + \dots \,;$$

In this expression, the stiffness of the Néel order is ρ_s, and $\chi_\perp$ is the uniform susceptibility transverse to the local Néel order. The coefficients are

$$
\begin{aligned}
\rho_s &= (J_1 - 2J_2 - 4J_3 + 10J_4)S^2 \\
\chi_\perp^{-1} &= 8(J_1 + 2J_4 - 4KS^2) \\
C_1 &= 16K, \quad C_2 = -\frac{(J_1 + 2J_2 + 4J_3 + 10J_4 - 8KS^2)}{2} \,.
\end{aligned}
\tag{A4}
$$

The quantum fluctuations of the spin S antiferromagnet are then described by the action [44]

$$\mathcal{S}_{\boldsymbol{n}} = \int dt d^2 r \left[\boldsymbol{L} \cdot (\boldsymbol{n} \times \partial_t \boldsymbol{n}) - \overline{\mathcal{H}}_J \right] + \mathcal{S}_B \tag{A5}$$

where $\mathcal{S}_B$ is as in Eq. (11) but now associated with 'hedgehog' defects in $\boldsymbol{n}$ [37–39].

The theory $\mathcal{S}_{\boldsymbol{n}}$ with only the first two terms in $\overline{\mathcal{H}}$ is the same [39] as the original $\mathbb{CP}^1$ model in Eq. (11), and so displays the phases D' (Néel) and D (VBS). Now consider the transition from D' to the spiral phase B': this occurs when increasing $J_{2,3}$ turns ρ_s negative, and we enter a state with $\langle \partial_a \boldsymbol{n} \rangle$ non-zero and spatially precessing; the pitch of the spiral is determined by higher order terms in Eq. (A3). Similarly, we transition from state D' to the canted state A' when $\chi_\perp^{-1}$ turns negative with increasing K: the state A' has $\langle \boldsymbol{L} \rangle \neq 0$, with a value stabilized by the quartic term C_1. Finally, the state C' has both $\langle \partial_a \boldsymbol{n} \rangle \neq 0$ and $\langle \boldsymbol{L} \rangle \neq 0$, and the second constraint in Eq. (A2) and $C_2 > 0$ lead to a conical spiral.

These considerations on the O(3) model can be connected to the $\mathbb{CP}^1$ analysis by the important identity (which follows from $\boldsymbol{n} = z_\alpha^* \boldsymbol{\sigma}_{\alpha\beta} z_\beta$ and $|z_\alpha|^2 = 1$)

$$(\partial_\mu \boldsymbol{n}) \cdot (\partial_\nu \boldsymbol{n}) = 2(\varepsilon_{\alpha\beta} z_\alpha \partial_\mu z_\beta)(\varepsilon_{\gamma\delta} z_\gamma^* \partial_\nu z_\delta^*) + \text{c.c.} . \tag{A6}$$

From Eq. (12) we therefore have the correspondence

$$(\partial_a \boldsymbol{n}) \cdot (\partial_b \boldsymbol{n}) \sim Q_a^* Q_b + Q_a Q_b^* \quad , \quad (\partial_t \boldsymbol{n}) \cdot (\partial_t \boldsymbol{n}) \sim |P|^2$$
$$(\partial_a \boldsymbol{n}) \cdot (\partial_t \boldsymbol{n}) \sim Q_a^* P + Q_a P^* . \tag{A7}$$

Using also $\partial_t \boldsymbol{n} \sim \boldsymbol{n} \times \boldsymbol{L}$ (from Eq. (A5)), we can now see that the identifications, in the previous paragraph, of the condensates in the O(3) model correspond to those of the $\mathbb{CP}^1$ model in Fig. 1a. The O(3) model analysis has located the phases of Fig. 1a in the parameter space of the lattice model $\mathcal{H}$, and we can also use it to estimate couplings in the $\mathbb{CP}^1$ theory.

Appendix B: Spin density wave theory

In this appendix, we study the fermionic Hubbard model on the square lattice using a mean-field approach, and show that metallic phases with all four spin-density wave orders discussed in the main text show up close to half-filling. We start with the Hubbard Hamiltonian for the electrons $c_{i,\alpha}$.

$$\mathcal{H}_U = - \sum_{i<j,\alpha} t_{ij} c_{i,\alpha}^\dagger c_{j,\alpha} - \mu \sum_{i,\alpha} c_{i,\alpha}^\dagger c_{i,\alpha} + U \sum_i \hat{n}_{i,\uparrow} \hat{n}_{i,\downarrow} \tag{B1}$$

where α is a spin-index, $t_{ij} = t_p$ are the hopping parameters for p'th nearest neighbors with $t_p \neq 0$ for $p = 1, 2, 3$ and 4, U is the Hubbard on-site repulsion and μ is the chemical potential. We perform a mean-field decoupling of the interaction term as follows [45–48]:

$$U\hat{n}_{i,\uparrow}\hat{n}_{i,\downarrow} = \frac{U}{4}\hat{n}_i^2 - U(\hat{\boldsymbol{S}}_i \cdot \boldsymbol{u}_i)^2 \rightarrow -\zeta_i \hat{n}_i - \boldsymbol{h}_i \cdot \hat{\boldsymbol{S}}_i - \frac{U}{4}\langle \hat{n}_i \rangle^2 + U\langle \hat{\boldsymbol{S}}_i \rangle^2 \tag{B2}$$

where $\hat{\boldsymbol{S}}_i = \frac{1}{2} c_{i,\alpha}^\dagger \boldsymbol{\sigma}_{\alpha\beta} c_{i,\beta}$ is the electron spin operator, $\hat{n}_i = \sum_\alpha \hat{n}_{i,\alpha}$ is the particle number operator at site $\boldsymbol{r}_i$, $\boldsymbol{u}_i$ is the unit-vector along the spin-quantization axis, $\zeta_i = -\frac{U}{2}\langle \hat{n}_i \rangle$ is a renormalization of the chemical potential which is henceforth absorbed in μ, and $\boldsymbol{h}_i = 2U\langle \hat{\boldsymbol{S}}_i \rangle$ is the mean magnetic field at site $\boldsymbol{r}_i$.

We consider states which are translation invariant in the charge sector. Therefore the charge density $\langle \hat{n}_i \rangle = n$ is the same on every site. We include the possibility of in-plane Néel and spiral order, as well as ferromagnetic canting in the orthogonal (z) direction:

$$\left\langle \hat{\boldsymbol{S}}_i \right\rangle = N_0 \left[\cos\left(\boldsymbol{K} \cdot \boldsymbol{r}_i \right) \cos(\theta)\, \hat{\boldsymbol{e}}_x + \sin\left(\boldsymbol{K} \cdot \boldsymbol{r}_i \right) \cos(\theta)\, \hat{\boldsymbol{e}}_y + \sin(\theta)\, \hat{\boldsymbol{e}}_z \right]. \tag{B3}$$

We expect that having the largest possible magnetization at each site will be energetically more favorable. Therefore, we have neglected the possibility of the collinear incommensurate state (stripes) as that leads to a variation in particle number density. While the Néel or spiral spin-density wave states can consistently explain the drop in Hall number and longitudinal conductivities in the cuprates [49–51], stripes seem to be inconsistent with the experimental data [52]. This provide additional motivation for restricting our study to the states described by Eq. (B3). The assumption of uniform charge density also rules out phase separation into hole-rich and particle-rich regions, which are often found
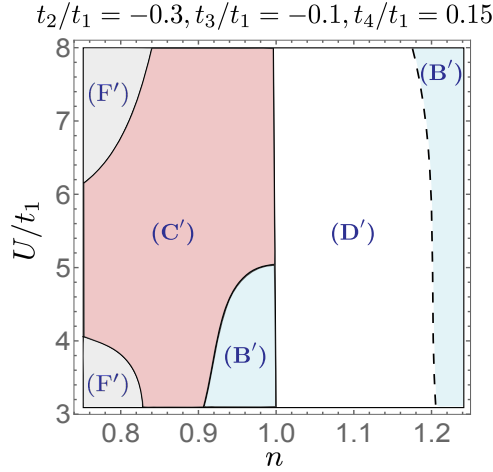
FIG. 3. Phase diagram from the spin-density wave analysis as a function of Hubbard U and doping n at fixed hopping, showing the Néel (D′), spiral (B′), conical spiral (C′) and ferromagnetic (F′) phases. As in Fig. 2, solid (dashed) lines are used to represent second (first) order transitions.

in such mean-field treatments [48]. In principle, farther interactions beyond a single on-site Hubbard repulsion can help avoid phase separation, but such physics cannot be captured by a mean-field treatment. Finally, we also do not consider possible superconductivity since we are interested in metallic phases (which appear at temperatures above the exponentially small superconducting T_c).

The mean-field grand canonical Hamiltonian can then be written in terms of a 2-component spinor $\Psi_{\boldsymbol{k}}$, the dispersion $\xi_{\boldsymbol{k}} = -\sum_{j \neq i} t_{ij} e^{i\boldsymbol{k} \cdot (\boldsymbol{r}_i - \boldsymbol{r}_j)} - \mu$, and $h = |\boldsymbol{h}_i| = 2UN_0$ as

$$\mathcal{H}_U^{MF} = \sum_{\boldsymbol{k}} C_{\boldsymbol{k}}^\dagger h_{\boldsymbol{k}} C_{\boldsymbol{k}}, \text{ where } h_{\boldsymbol{k}} = \begin{pmatrix} \xi_{\boldsymbol{k}} - \frac{h}{2}\sin\theta & -\frac{h}{2}\cos\theta \\ -\frac{h}{2}\cos\theta & \xi_{\boldsymbol{k}+\boldsymbol{K}} + \frac{h}{2}\sin\theta \end{pmatrix}, \text{ and } C_{\boldsymbol{k}} = \begin{pmatrix} c_{\boldsymbol{k},\uparrow} \\ c_{\boldsymbol{k}+\boldsymbol{K},\downarrow} \end{pmatrix}. \tag{B4}$$

This can be diagonalized by a unitary transformation

$$\begin{pmatrix} c_{\boldsymbol{k},\uparrow} \\ c_{\boldsymbol{k}+\boldsymbol{K},\downarrow} \end{pmatrix} = \begin{pmatrix} \cos\phi_{\boldsymbol{k}} & \sin\phi_{\boldsymbol{k}} \\ -\sin\phi_{\boldsymbol{k}} & \cos\phi_{\boldsymbol{k}} \end{pmatrix} \begin{pmatrix} \alpha_{\boldsymbol{k}} \\ \beta_{\boldsymbol{k}} \end{pmatrix}, \text{ where } \tan(2\phi_{\boldsymbol{k}}) = \frac{h\cos\theta}{\xi_{\boldsymbol{k}} - \xi_{\boldsymbol{k}+\boldsymbol{K}} - h\sin\theta} \tag{B5}$$

The energies of the upper and lower Hubbard bands are given by ($s = \pm$)

$$E_{\boldsymbol{k},s} = \frac{1}{2}\left(\xi_{\boldsymbol{k}} + \xi_{\boldsymbol{k}+\boldsymbol{K}} + s\sqrt{(\xi_{\boldsymbol{k}} - \xi_{\boldsymbol{k}+\boldsymbol{K}} - h\sin\theta)^2 + h^2\cos^2\theta}\right). \tag{B6}$$

The free energy of the system in the canonical ensemble is given in the continuum limit by (setting N_s to be the number of lattice sites)

$$\frac{E^{MF}}{N_s} = \sum_{s=\pm}\int \frac{d^2k}{(2\pi)^2} E_{\boldsymbol{k},s}\, n_F(E_{\boldsymbol{k},s}) + \mu n - \frac{Un^2}{4} + \frac{h^2}{4U}, \text{ where } n = \langle \hat{n}_i \rangle = \sum_{s=\pm}\int \frac{d^2k}{(2\pi)^2} n_F(E_{\boldsymbol{k},s}).$$

We first tune μ to adjust the electron-filling n. At a fixed filling, we minimize the mean-field free energy $E^{MF}(h,\theta,\boldsymbol{K})$. The values of these parameters at the minima in turn describe the magnetically ordered (or paramagnetic) phase for a given set of hopping parameters t_p and Hubbard repulsion U.

As shown in Fig. 2 in the main text and in Fig. 3 in this appendix, at large U we find exactly the 4 kinds of spin-density wave phases (D′) $\boldsymbol{K} = (\pi, \pi)$, $\theta = 0$, (A′) $\boldsymbol{K} = (\pi, \pi)$, $0 < \theta < \pi/2$, (B′) $\boldsymbol{K}$ incommensurate, $\theta = 0$, and (C′) $\boldsymbol{K}$ incommensurate, $0 < \theta < \pi/2$. As expected, in the insulator ($n = 1$) the nearest neighbor Heisenberg exchange J_1 is dominant at large U, and we find the insulator to be always in the Néel phase (D′). In the metallic states, the Néel phase only appears close to zero doping, while the other three antiferromagnetic phases appear contiguous to the Néel phase. The presence of t_p for $p > 1$ breaks particle-hole symmetry. It is interesting to note that the canted phases appear only on the hole-doped side ($n < 1$) while the electron-doped side has coplanar magnetic order (even at larger dopings not shown in Figs. 2 and 3). Finally, an additional ferromagnetic phase (F') with $\theta = \pi/2$ also shows up at low enough hole-doping, consistent with previous mean-field studies of the Hubbard model [47, 48].

Appendix C: SU(2) gauge theory

In this appendix, we derive the effective chargon Hamiltonian (9) from the Hubbard model in Eq. (3) and study the symmetries, together with the associated current and bond patterns, of the different Higgs-field configurations stated in the main text.

1. Effective chargon Hamiltonian

We write the Hubbard Hamiltonian $\mathcal{H}_U$ as a coherent state path integral and decouple the interaction using a Hubbard-Stratonovich field $\boldsymbol{\Phi}_i$. This yields the equivalent action $\mathcal{S} = \mathcal{S}_c + \mathcal{S}_{\text{int}} + \mathcal{S}_\Phi$, where ($\beta$ and τ denote inverse temperature and imaginary time, respectively)

$$\mathcal{S}_c = \int_0^\beta d\tau \left[\sum_{i,\alpha} c_{i,\alpha}^\dagger (\partial_\tau - \mu) c_{i,\alpha} - \sum_{i<j,\alpha} t_{ij} c_{i,\alpha}^\dagger c_{j,\alpha} \right] \tag{C1}$$

describes the hopping of the electrons on the square lattice; The electrons are coupled to the Hubbard-Stratonovich field via

$$\mathcal{S}_{\text{int}} = \int_0^\beta d\tau \sum_i c_{i,\alpha}^\dagger \boldsymbol{\sigma}_{\alpha\beta} c_{,i\beta} \cdot \boldsymbol{\Phi}_i \tag{C2}$$

and the action of $\boldsymbol{\Phi}_i$ reads as

$$\mathcal{S}_\Phi = \frac{3}{2U} \int_0^\beta d\tau \sum_i \boldsymbol{\Phi}_i^2. \tag{C3}$$

We next transform the electrons to a rotating reference frame as defined in Eq. (4). To rewrite the action in terms of the new degrees of freedom, the chargon and spinon fields ψ_i and R_i, let us first focus on $\mathcal{S}_c$. The hopping terms assume the form

$$\sum_\alpha t_{ij} c_{i,\alpha}^\dagger c_{j,\alpha} = \sum_{s,s',\beta} t_{ij} \psi_{i,s}^\dagger \left(R_i^\dagger \right)_{s\beta} (R_j)_{\beta s'} \psi_{j,s'} \tag{C4}$$

using $\alpha, \beta = \uparrow, \downarrow$ and $s, s' = \pm$ as physical spin and SU(2)-gauge indices, respectively. To make the quartic term accessible analytically, we perform a mean-field decoupling. Upon introducing $(U_{ij})_{ss'} = \langle (R_i^\dagger R_j)_{ss'} \rangle$ and $(\chi_{ij})_{ss'} = \langle \psi_{i,s}^\dagger \psi_{j,s'} \rangle$, Eq. (C4) becomes

$$t_{ij} \sum_{s,s'} \left(\psi_{i,s}^\dagger (U_{ij})_{ss'} \psi_{j,s'} + (\chi_{ij})_{ss'} \left(R_i^\dagger R_j \right)_{ss'} \right). \tag{C5}$$

In the same way, we can rewrite and decouple the time-derivative and chemical potential terms in Eq. (C1).

Introducing the 'Higgs' field $\boldsymbol{H}_i$ according to (cf. Eq. (5))

$$\boldsymbol{\sigma} \cdot \boldsymbol{H}_i = R_i^\dagger \boldsymbol{\sigma} R_i \cdot \boldsymbol{\Phi}_i, \tag{C6}$$

the remaining parts of the action, $\mathcal{S}_{\text{int}}$ and $\mathcal{S}_\Phi$, can be restated as

$$\mathcal{S}_{\text{int}} = \int_0^\beta d\tau \, \boldsymbol{H}_i \cdot \sum_{i,s,s'} \psi_{i,s}^\dagger \boldsymbol{\sigma}_{ss'} \psi_{i,s'}, \tag{C7}$$

$$\mathcal{S}_\Phi = \frac{3}{2U} \int_0^\beta d\tau \sum_i \boldsymbol{H}_i^2. \tag{C8}$$

Taken together, the new action consists of three parts: The effective chargon action,

$$\mathcal{S}_\psi = \int_0^\beta d\tau \left[\sum_{i,s} \psi_{i,s}^\dagger (\partial_\tau - \mu) \psi_{i,s} - \sum_{i<j,s,s'} t_{ij} \psi_{i,s}^\dagger (U_{ij})_{ss'} \psi_{j,s'} \right.$$
$$\left. + \sum_{i,s,s'} \boldsymbol{H}_i \cdot \psi_{i,s}^\dagger \boldsymbol{\sigma}_{ss'} \psi_{i,s'} \right], \tag{C9}$$

the spinon action (tr denotes the trace in SU(2) space),

$$\mathcal{S}_R = \int_0^\beta d\tau \, \mathrm{tr} \left[\sum_i \chi_{ii}^T R_i^\dagger \partial_\tau R_i - \sum_{i,j} t_{ij} \chi_{ij}^T R_i^\dagger R_j \right], \tag{C10}$$

which will be discussed in detail in Appendix D below, and the bare Higgs action in Eq. (C8).

Let us for now assume that U_{ij} in Eq. (C9) is trivial in SU(2) space, $(U_{ij})_{ss'} = Z_{ij}\delta_{ss'}$. This should be seen as the first step in or the 'ansatz' for an iterative self-consistent calculation of χ_{ij} and U_{ij} where these two quantities are inserted in and calculated from the spinon and chargon actions until convergence is reached. At the end of this appendix, we will show that there are no qualitative changes when the self-consistent iterations are carried out.

For $(U_{ij})_{ss'} = Z_{ij}\delta_{ss'}$, we recover the effective chargon Hamiltonian (9) stated in the main text. Furthermore, the bare Higgs field action and the coupling of the Higgs to the chargons is mathematically equivalent to the bare action of the Hubbard-Stratonovich field $\boldsymbol{\Phi}_i$ and its coupling to the electrons. For this reason, we can directly transfer the results of the spin-density-wave calculation of Appendix B to the Higgs phase. The main modification is an order-one rescaling of the hopping parameters from the bare electronic values t_{ij} to those of the chargons $Z_{ij}t_{ij}$.

2. Symmetries and current patterns

Let us next analyze the symmetries of the effective chargon Hamiltonian (9) for the different Higgs condensates parameterized in Eq. (8) of the main text.

As a consequence of the SU(2) gauge redundancy, a lattice symmetry g with real space action $i \to g(i)$ is preserved if and only if there are SU(2) matrices $G_i(g)$ such that the effective chargon Hamiltonian is invariant under

$$\psi_{i,s} \to \sum_{s'} (G_i(g))_{s,s'} \, \psi_{g(i),s'}. \tag{C11}$$

To illustrate the nontrivial consequences of the additional gauge degree of freedom, let us consider translation symmetry $g = T_\mu$, $\mu = x, y$, with $T_\mu(i) = i + \hat{\boldsymbol{e}}_\mu$. We first note that all configurations in Eq. (8) satisfy

$$\langle \boldsymbol{H}_{i+\boldsymbol{e}_\mu} \rangle = \begin{pmatrix} R(K_\mu) & \begin{matrix} 0 \\ 0 \end{matrix} \\ 0 \;\; 0 & 1 \end{pmatrix} \langle \boldsymbol{H}_i \rangle, \tag{C12}$$

where $R(\varphi)$ is a 2×2 matrix describing the rotation of 2D vectors by angle φ. As the matrix in Eq. (C12) belongs to SO(3) and the Higgs field transforms under the adjoint representation of SU(2), we can always find $G_i(T_\mu)$ to render the chargon Hamiltonian invariant; Translation symmetry is thus preserved in all Higgs phases discussed in the main text.

To present an example of broken translation symmetry, let us consider the 'staggered conical spiral', labeled by $(\mathrm{E})_{\boldsymbol{K}}^{(\eta_x,\eta_y)}$, $\eta_\mu = \pm 1$, in the following, where with $\boldsymbol{r}_i = (i_x, i_y)$

$$\langle \boldsymbol{H}_i \rangle = H_0 \left[\cos(\boldsymbol{K} \cdot \boldsymbol{r}_i) \cos(\theta) \, \hat{\boldsymbol{e}}_x + \sin(\boldsymbol{K} \cdot \boldsymbol{r}_i) \cos(\theta) \, \hat{\boldsymbol{e}}_y + \eta_x^{i_x} \eta_y^{i_y} \sin(\theta) \, \hat{\boldsymbol{e}}_z \right], \tag{C13}$$

with at least one of η_x, η_y equal to -1, $0 < \theta < \pi/2$, and incommensurate $\boldsymbol{K}$. We chose this particular example since we have found the associated magnetically ordered phase as the ground state in the classical analysis of the spin model in Eq. (2). It is not visible in Fig. 2(a)–(c) as it only appears for larger values of J_2. For this configuration, the 1 in the matrix in Eq. (C12) has to be replaced by η_μ. If $\eta_\mu = -1$, the matrix in Eq. (C12) has determinant -1 and, hence, does not belong to SO(3). Consequently, translation symmetry along μ is broken if $\eta_\mu = -1$. Note that ΘT_μ, with Θ denoting time-reversal, is still a symmetry since the Higgs field is odd under Θ.

Similarly, time-reversal and all other lattice symmetries of the effective chargon Hamiltonian can be analyzed. The result is summarized in Table II where the residual symmetries of all the phases with $\mathbb{Z}_2$ topological order discussed in the main text are listed. Note that time-reversal-symmetry breaking necessarily requires a non-collinear Higgs phase since, otherwise, $\boldsymbol{H}_i \to -\boldsymbol{H}_i$ can be undone by a global gauge transformation (a global rotation of the Higgs field).

A complementary and physically insightful approach of detecting and visualizing broken symmetries is based on calculating the (time-reversal symmetric) kinetic energies K_{ij} and the (time-reversal odd) currents J_{ij} on the different bonds (i,j) of the lattice in the ground state of the chargon Hamiltonian. These two quantities are defined as and calculated from $K_{ij} = -2\mathrm{Re}\, T_{ij}$ and $J_{ij} = 2\mathrm{Im}\, T_{ij}$ where

$$T_{ij} = Z_{ij} t_{ij} \sum_s \langle \psi_{i,s}^\dagger \psi_{j,s} \rangle_{\langle \boldsymbol{H}_i \rangle}. \tag{C14}$$

TABLE II. Generators of the residual symmetry group of the Higgs phases with $\mathbb{Z}_2$ topological order shown in Fig. 1b of the main text. We use Θ to denote time-reversal, C_n for n-fold rotation along the z axis. I_x (I_y) and $I_\pm$ are the reflections with action $x \to -x$ ($y \to -y$) and at the plane spanned by $x = \pm y$ and the z axis, respectively.

Higgs Phase	Residual generators
(A)	T_μ, C_4, I_y, Θ
(B)$_{(k,\pi)}$/(B)$_{(\pi,k)}$	T_μ, C_2, I_y, Θ
(B)$_{(k,k)}$/(B)$_{(k,-k)}$	T_μ, C_2, I_+, Θ
(C)$_{(k,\pi)}$/(C)$_{(\pi,k)}$	T_μ, ΘC_2, $I_{y/x}$
(C)$_{(k,k)}$/(C)$_{(k,-k)}$	T_μ, ΘC_2, $I_{+/-}$

$(\mathbf{E})^{(+,-)}_{(k,\pi)}$

$(\mathbf{E})^{(+,-)}_{(k,k)}$ $\quad (\mathbf{E})^{(+,-)}_{(k,-k)}$

$(\mathbf{E})^{(-,-)}_{(k,\pi)}$
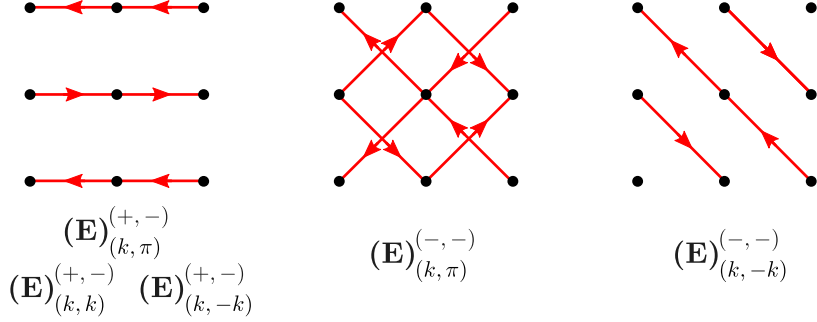
$(\mathbf{E})^{(-,-)}_{(k,-k)}$

FIG. 4. Bond currents (arrows) are shown for the different (symmetry inequivalent) staggered conical spiral Higgs field configurations that allow for finite currents in a model with only nearest and next-to-nearest neighbor hopping on the square lattice (dots).

Here $\langle \dots \rangle_{\langle \boldsymbol{H}_i \rangle}$ denotes the expectation values with respect to the ground state of the chargon Hamiltonian $\mathcal{H}_\psi$ in Eq. (9) for a given Higgs condensate $\boldsymbol{H}_i \to \langle \boldsymbol{H}_i \rangle$. The kinetic energies K_{ij} (black solid and dashed lines) and, if finite, the currents J_{ij} (black arrows) along the different bonds are illustrated in Fig. 1(b) for the three different phases (A)–(C) with $\mathbb{Z}_2$ topological order focussing on a model where only the nearest t_1 and next-to-nearest neighbor hopping t_2 are non-zero.

For completeness, we also illustrate the current patterns for the staggered conical spiral phases in Fig. 4. Here, four unit cells of the square lattice are shown as translation by one lattice site T_μ is broken if $\eta_\mu = -1$ while T_μ^2 is preserved.

Three comments on the staggered conical spiral configurations are in order. We first note that the (magnetic) point symmetries of $(E)^{(\eta_x, \eta_y)}_{(k,\pi)}$ and $(E)^{(\eta,\eta)}_{(k,k)}$ are the same as those of $(C)_{(k,\pi)}$ and $(C)_{(k,k)}$, given in Table II, while $(E)^{(\eta,-\eta)}_{(k,k)}$ only has ΘC_2 symmetry. Secondly, the nearest neighbor current operator $J_{i,i+\hat{\boldsymbol{e}}_\mu}$ must be zero if $\eta_\mu = -1$ since the residual symmetry ΘC_2 implies $J_{i,i+\hat{\boldsymbol{e}}_\mu} = J_{i-\hat{\boldsymbol{e}}_\mu,i}$ while ΘT_μ leads to $J_{i,i+\hat{\boldsymbol{e}}_\mu} = -J_{i-\hat{\boldsymbol{e}}_\mu,i}$. For the same reason, we conclude that the diagonal currents must vanish if $\eta_x \eta_y = -1$. Third, notice that the configuration $(E)^{(+,-)}_{(\pi,k)}$ cannot support finite currents in the model with nearest and next-to-nearest-neighbor hopping since the (magnetic) point symmetries and the (magnetic) translations are only consistent with $J_{ij} = 0$ along all bonds of the lattice (Finite currents are possible in the presence of third-nearest-neighbor hopping. The associated current pattern is not shown in Fig. 4).

Finally, let us come back to the issue of calculating U_{ij} (and χ_{ij} entering the spinon action) self-consistently. While we had used the ansatz of diagonal U_{ij} for the iteration, recalculating U_{ij} from the spinon action will in general also yield non-vanishing off-diagonal components; However, the symmetry analysis we discussed above is not affected since symmetries are preserved in the iteration process. To see this, assume that the chargon Hamiltonian $\mathcal{H}_\psi[\boldsymbol{H}_i, U_{ij}^{(0)}]$ with a certain Higgs field configuration $\boldsymbol{H}_i$ and gauge connection $U_{ij} = U_{ij}^{(0)}$ (e.g., $U_{ij}^{(0)} = Z_{ij}\sigma_0$ in the first iteration) is invariant under a symmetry operation g, i.e., invariant under (C11). This implies that the χ_{ij} calculated from $\mathcal{H}_\psi[\boldsymbol{H}_i, U_{ij}^{(0)}]$ satisfy $\chi_{ij} = G_i^*(g)\chi_{g(i)g(j)}G_j^T(g)$. Consequently, the spinon action in Eq. (C10) is symmetric under $R_i \to R_{g^{-1}(i)}G_{g^{-1}(i)}(g)$, where g^{-1} denotes the inverse of g. The 'new' or 'updated' gauge connection $U_{ij} = U_{ij}^{(1)}$ as

obtained from the spinon action thus satisfies

$$U^{(1)}_{g(i)g(j)} = G^\dagger_i(g)U^{(1)}_{ij}G_j(g) \tag{C15}$$

and, hence, the 'new' chargon Hamiltonian $\mathcal{H}_\psi[\boldsymbol{H}_i, U^{(1)}_{ij}]$ is still invariant under (C11). This means that the symmetries and the qualitative form of the bond as well as current patterns discussed above are unaffected by replacing $U_{ij} = U^{(0)}_{ij} = Z_{ij}\sigma_0$ by the, generally non-diagonal, self-consistent solution U_{ij} obtained via iteration. The off-diagonal components in U_{ij} should be seen as additional corrections to the energetics of the spin-density-wave analysis of Appendix B and, hence, are expected to only lead to small changes in the phase boundaries in Fig. 2d-f.

Appendix D: Derivation of $\mathbb{CP}^1$ theory from SU(2) gauge theory

To derive the $\mathbb{CP}^1$ actions for the different phases in Fig. 1b from the SU(2) gauge theory, it is convenient to use the gauge where the Higgs field is given by

$$\langle \boldsymbol{H}_i \rangle = (-1)^{i_x+i_y} H_0 \,\hat{\boldsymbol{e}}_z, \tag{D1}$$

i.e., the Higgs field has the form of the spin configuration of an antiferromagnet. Choosing the 'antiferromagnetic gauge' in Eq. (D1) is possible for all configurations in Eq. (8) or, more generally, in Eq. (C13), since the Higgs field transforms under the adjoint representation of SU(2) and $|\langle \boldsymbol{H}_i \rangle| = H_0$.

In this gauge, the relation between the $\mathbb{CP}^1$ fields $z_i = (z_{i\uparrow}, z_{i\downarrow})$ and the spinons R_i is given by Eq. (10) for all Higgs configurations. This is verified by noting that Eq. (5) with $\hat{\boldsymbol{S}}_i = (-1)^{i_x+i_y}\boldsymbol{n_i}$ and $\boldsymbol{n_i} = z^\dagger_i\boldsymbol{\sigma}z_i$ will hold for R_i given in Eq. (10) if the Higgs field has the form (D1). As R_i transforms nontrivially under SU(2) gauge transformations, see Eq. (6), the relation between z_i and R_i is generally different in a different gauge.

Inserting the parameterization (10) into Eq. (C10) and writing $\chi^{ss'}_{ij} = (\chi_{ij})_{ss'}$ yields the general form

$$\mathcal{S}_z = \int_0^\beta d\tau \Bigg[\sum_i \Big((\chi^{++}_{ii} - \chi^{--}_{ii})z^\dagger_i\partial_\tau z_i + \chi^{-+}_{ii}\varepsilon_{\alpha\beta}z_{i,\alpha}\partial_\tau z_{i,\beta} - \chi^{+-}_{ii}\varepsilon_{\alpha\beta}z^*_{i,\alpha}\partial_\tau z^*_{i,\beta} \Big)$$
$$- \sum_{i<j} t_{ij}\Big((\chi^{++}_{ij} + \chi^{--}_{ji})z^\dagger_i z_j + (\chi^{-+}_{ij} - \chi^{-+}_{ji})\varepsilon_{\alpha\beta}z_{i,\alpha}z_{j,\beta} + \text{c.c.} \Big) \Bigg], \tag{D2}$$

of the $\mathbb{CP}^1$ action. We already notice (the lattice form of) the charge-2 terms $\varepsilon_{\alpha\beta}z_\alpha\partial_\tau z_\beta$ and $\varepsilon_{\alpha\beta}z_\alpha\partial_a z_\beta$, $a = x, y$, coupling to the Higgs fields P and Q_a in Eq. (13).

Depending on the symmetries of the chargon Hamiltian, some of the terms in Eq. (D2) have to vanish as we will discuss next. This corresponds to the absence of condensation of one or both of the Higgs fields P and Q_a in the phases (A), (B), and (D).

Since this has already been discussed for the case of phase (D) in Ref. 53, we focus here on the other three cases. To begin with phase (B), we apply the gauge transformation $V_i = e^{-i\pi\sigma_y/4}e^{i\delta\boldsymbol{K}\cdot\boldsymbol{r}_i\sigma_x/2}$, where $\delta\boldsymbol{K} = \boldsymbol{K} - (\pi,\pi)$, to bring the associated Higgs field configuraton in the form of Eq. (D1). In the resulting 'antiferromagnetic gauge', the chargon Hamiltonian reads as

$$\mathcal{H}^{(B)}_\psi = -\sum_{i<j,s,s'} t_{ij}Z_{ij}\psi^\dagger_{i,s}\left(e^{i\delta\boldsymbol{K}\cdot(\boldsymbol{r}_j-\boldsymbol{r}_i)\frac{\sigma_x}{2}}\right)_{ss'}\psi_{j,s'} - \mu\sum_{i,s}\psi^\dagger_{i,s}\psi_{i,s} - H_0\sum_{i,s}(-1)^{i_x+i_y}s\,\psi^\dagger_{i,s}\psi_{i,s}. \tag{D3}$$

We see that $\boldsymbol{K} \neq (\pi,\pi)$, *i.e.*, $\delta\boldsymbol{K} \neq 0$, is required to have off-diagonal matrix elements in SU(2) space ($s \neq s'$) in the Hamiltonian. These are necessary for charge-2 terms in the $\mathbb{CP}^1$ action as otherwise $\chi^{s;-s}_{ij} = 0$ and, hence, the prefactors of $\varepsilon_{\alpha\beta}z_{i,\alpha}\partial_\tau z_{i,\beta}$ and $\varepsilon_{\alpha\beta}z_{i,\alpha}z_{j,\beta}$ vanish in Eq. (D2). Alternatively, this can also be seen by noting that $R_iV^\dagger_i = R_i|_{z_i\to z_ie^{i\xi}}$ for the global gauge transformation $V_i = e^{-i\xi\sigma_z}$ and that all terms in the chargon Hamiltonian $\mathcal{H}^{(B)}_\psi$ are invariant under this gauge transformation, $\psi_i \to V_i\psi_i$, except for the contributions of finite $\delta\boldsymbol{K}$ to the hopping term. This means that the effective $\mathbb{CP}^1$ action must be invariant under $z_i \to z_ie^{i\xi}$ in the limit $\delta\boldsymbol{K} = 0$, *i.e.*, the charge-2 terms can only arise if $\delta\boldsymbol{K} \neq 0$.

To see which of the two possible charge-2 terms in Eq. (D2) can be non-zero, let us analyze the symmetries of the chargon Hamiltonian $\mathcal{H}^{(B)}_\psi$ for non-zero $\delta\boldsymbol{K}$. We first note that $\mathcal{H}^{(B)}_\psi$ is invariant under $\psi_{i,s} \to \psi_{i+\hat{\boldsymbol{e}}_\mu,-s}$ leading to

$$\chi^{ss'}_{ij} = \chi^{-s-s'}_{i+\hat{\boldsymbol{e}}_\mu j+\hat{\boldsymbol{e}}_\mu} = \chi^{ss'}_{i+2\hat{\boldsymbol{e}}_\mu j+2\hat{\boldsymbol{e}}_\mu}. \tag{D4}$$

From this follows

$$\chi_{ii}^{++} - \chi_{ii}^{--} = \chi_{ii}^{++} - \chi_{i+\hat{e}_\mu i+\hat{e}_\mu}^{++} = (-1)^{i_x+i_y}\chi_\tau. \tag{D5}$$

The constant χ_τ can be shown to be real: The Hamiltonian $\mathcal{H}_\psi^{(B)}$ commutes with the antiunitary operator $\widetilde{\Theta}$ defined by $\widetilde{\Theta}\psi_{j,s}\widetilde{\Theta}^\dagger = i\sigma_z\psi_{j,s}$. This implies

$$\chi_{ij}^{ss'} = ss'\left(\chi_{ij}^{ss'}\right)^* = ss'\chi_{ji}^{s's}. \tag{D6}$$

This not only leads to $\chi_\tau \in \mathbb{R}$, but can also be used to rewrite

$$\chi_{ij}^{++} + \chi_{ji}^{--} = \chi_{ij}^{++} + \chi_{i+\hat{e}_\mu j+\hat{e}_\mu}^{++} = \chi_{i-j}^t \in \mathbb{R}, \tag{D7a}$$

$$\chi_{ij}^{-+} - \chi_{ji}^{-+} = \chi_{ij}^{-+} + \chi_{i+\hat{e}_\mu j+\hat{e}_\mu}^{-+} = \chi_{i-j}^Q = -\chi_{j-i}^Q \in i\mathbb{R}, \tag{D7b}$$

where we have also taken advantage of Eq. (D4).

We finally consider the symmetry of $\mathcal{H}_\psi^{(B)}$ under the unitary transformation $\psi_{j,s} \to i\sigma_z\psi_{-j,s}$ which, together with Eq. (D4), leads to

$$\chi_{ii}^{+-} = -\chi_{-i-i}^{+-} = -\chi_{ii}^{+-} = 0. \tag{D8}$$

Consequently, the terms $\varepsilon_{\alpha\beta}z_{i,\alpha}\partial_\tau z_{i,\beta}$ and $\varepsilon_{\alpha\beta}z_{i,\alpha}^*\partial_\tau z_{i,\beta}^*$ are absent in Eq. (D2) for phase (B).

Taken together, the $\mathbb{CP}^1$ action $\mathcal{S}_z$ in Eq. (D2) assumes the form

$$\mathcal{S}_z^{(B)} = \int_0^\beta d\tau\left[\sum_i (-1)^{i_x+i_y}\chi_\tau z_i^\dagger \partial_\tau z_i - \sum_{i<j} t_{ij}\left(\chi_{i-j}^t z_i^\dagger z_j + \chi_{i-j}^Q \varepsilon_{\alpha\beta}z_{i,\alpha}z_{j,\beta} + \text{c.c.}\right)\right]. \tag{D9}$$

For concreteness, let us focus on nearest-neighbor hopping ($t = t_{i,i+\hat{e}_\mu}$) and $\delta Q_x = \delta Q_y$ (corresponding to phase $(B)_{(k,k)}$). Using that $\chi_{\hat{e}_x}^{t,Q} = \chi_{\hat{e}_y}^{t,Q} \equiv i\chi^{Q,t}$, treating the constraint $z_i^\dagger z_i = 1$ on average by introducing the Lagrange multiplier λ, and rewriting

$$z_{i\alpha} \sim z_\alpha(\boldsymbol{r}_i) + (-1)^{i_x+i_y}\pi_\alpha(\boldsymbol{r}_i), \tag{D10}$$

where $z(\boldsymbol{r})$ and $\pi(\boldsymbol{r})$ are assumed to be slowly varying continuum fields, a gradient expansion of Eq. (D9) yields (a denotes lattice spacing)

$$\mathcal{S}_z^{(B)} \sim \int_0^\beta d\tau \int \frac{d^2r}{a^2}\left[\chi_\tau(z^\dagger\partial_\tau\pi + \pi^\dagger\partial_\tau z) + (\lambda - t\chi^t)z^\dagger z + (\lambda + t\chi^t)\pi^\dagger\pi \right.$$
$$\left. + t\chi^t a^2 \sum_{\mu=x,y}(\partial_\mu z^\dagger)\partial_\mu z + 2t\chi^Q a \sum_{\mu=x,y}(\varepsilon_{\alpha\beta}z_\alpha\partial_\mu z_\beta + \text{c.c})\right]. \tag{D11}$$

In Eq. (D11) spatial derivatives up to second (zeroth) order of z_α (π_α) are kept as these gives rise to the terms of the $\mathbb{CP}^1$ action we are interested in. Indeed, integrating out the π field, we recover the $\mathbb{CP}^1$ theory of the main text with Higgs condensates $\langle Q_x\rangle = \langle Q_y\rangle \neq 0$ and $\langle P\rangle = 0$.

In a similar way, the remaining phases, (A) and (C), can be analyzed and one finds the $\mathbb{CP}^1$ action with Higgs condensates summarized in Fig. 1b.

---

[1] J. M. Luttinger and J. C. Ward, "Ground-State Energy of a Many-Fermion System. II," Phys. Rev. **118**, 1417 (1960).

[2] B. Keimer, S. A. Kivelson, M. R. Norman, S. Uchida, and J. Zaanen, "From quantum matter to high-temperature superconductivity in copper oxides," Nature **518**, 179 (2015), arXiv:1409.4673 [cond-mat.supr-con].

[3] S. Badoux, W. Tabis, F. Laliberté, G. Grissonnanche, B. Vignolle, D. Vignolles, J. Béard, D. A. Bonn, W. N. Hardy, R. Liang, N. Doiron-Leyraud, L. Taillefer, and C. Proust, "Change of carrier density at the pseudogap critical point of a cuprate superconductor," Nature **531**, 210 (2016), arXiv:1511.08162 [cond-mat.supr-con].

[4] T. Senthil, S. Sachdev, and M. Vojta, "Fractionalized Fermi Liquids," Phys. Rev. Lett. **90**, 216403 (2003), cond-mat/0209144.

[5] T. Senthil, M. Vojta, and S. Sachdev, "Weak magnetism and non-Fermi liquids near heavy-fermion critical points," Phys. Rev. B **69**, 035111 (2004), cond-mat/0305193.

[6] A. Paramekanti and A. Vishwanath, "Extending Luttinger's theorem to $\mathbb{Z}_2$ fractionalized phases of matter," Phys. Rev. B **70**, 245118 (2004), cond-mat/0406619.

[7] Y. Ando, K. Segawa, S. Komiya, and A. N. Lavrov, "Electrical Resistivity Anisotropy from Self-Organized One Dimensionality in High-Temperature Superconductors," Phys. Rev. Lett. **88**, 137005 (2002), cond-mat/0108053.

[8] V. Hinkov, D. Haug, B. Fauqué, P. Bourges, Y. Sidis, A. Ivanov, C. Bernhard, C. T. Lin, and B. Keimer, "Electronic Liquid Crystal State in the High-Temperature Superconductor $YBa_2Cu_3O_{6.45}$," Science **319**, 597 (2008).

[9] R. Daou, J. Chang, D. Leboeuf, O. Cyr-Choinière, F. Laliberté, N. Doiron-Leyraud, B. J. Ramshaw, R. Liang, D. A. Bonn, W. N. Hardy, and L. Taillefer, "Broken rotational symmetry in the pseudogap phase of a high-T_c superconductor," Nature **463**, 519 (2010), arXiv:0909.4430 [cond-mat.supr-con].

[10] M. J. Lawler, K. Fujita, J. Lee, A. R. Schmidt, Y. Kohsaka, C. K. Kim, H. Eisaki, S. Uchida, J. C. Davis, J. P. Sethna, and E.-A. Kim, "Intra-unit-cell electronic nematicity of the high-T_c copper-oxide pseudogap states," Nature **466**, 347 (2010), arXiv:1007.3216 [cond-mat.supr-con].

[11] J. Xia, E. Schemm, G. Deutscher, S. A. Kivelson, D. A. Bonn, W. N. Hardy, R. Liang, W. Siemons, G. Koster, M. M. Fejer, and A. Kapitulnik, "Polar Kerr-Effect Measurements of the High-Temperature $YBa_2Cu_3O_{6+x}$ Superconductor: Evidence for Broken Symmetry near the Pseudogap Temperature," Phys. Rev. Lett. **100**, 127002 (2008), arXiv:0711.2494 [cond-mat.supr-con].

[12] Y. Lubashevsky, L. Pan, T. Kirzhner, G. Koren, and N. P. Armitage, "Optical Birefringence and Dichroism of Cuprate Superconductors in the THz Regime," Phys. Rev. Lett. **112**, 147001 (2014), arXiv:1310.2265 [cond-mat.str-el].

[13] L. Mangin-Thro, Y. Sidis, A. Wildes, and P. Bourges, "Intra-unit-cell magnetic correlations near optimal doping in $YBa_2Cu_3O_{6.85}$," Nature Communications **6**, 7705 (2015), arXiv:1501.04919 [cond-mat.supr-con].

[14] L. Zhao, C. A. Belvin, R. Liang, D. A. Bonn, W. N. Hardy, N. P. Armitage, and D. Hsieh, "A global inversion-symmetry-broken phase inside the pseudogap region of $YBa_2Cu_3O_y$," Nature Physics **13**, 250 (2017), arXiv:1611.08603 [cond-mat.str-el].

[15] A. Pal, S. R. Dunsiger, K. Akintola, A. C. Y. Fang, A. Elhosary, M. Ishikado, H. Eisaki, and J. E. Sonier, "Quasi-Static Internal Magnetic Field Detected in the Pseudogap Phase of $Bi_{2+x}Sr_{2-x}CaCu_2O_{8+\delta}$ by μSR," ArXiv e-prints (2017), arXiv:1707.01111 [cond-mat.supr-con].

[16] T. P. Croft, E. Blackburn, J. Kulda, R. Liang, D. A. Bonn, W. N. Hardy, and S. M. Hayden, "No Evidence for Orbital Loop Currents in Charge Ordered $YBa_2Cu_3O_{6+x}$ from Polarized Neutron Diffraction," ArXiv e-prints (2017), arXiv:1709.06128 [cond-mat.supr-con].

[17] S. Sachdev and N. Read, "Large N expansion for frustrated and doped quantum antiferromagnets," Int. J. Mod. Phys. B **5**, 219 (1991), cond-mat/0402109.

[18] M. Barkeshli, H. Yao, and S. A. Kivelson, "Gapless spin liquids: Stability and possible experimental relevance," Phys. Rev. B **87**, 140402 (2013), arXiv:1208.3869 [cond-mat.str-el].

[19] S. Chatterjee and S. Sachdev, "Insulators and metals with topological order and discrete symmetry breaking," Phys. Rev. B **95**, 205133 (2017), arXiv:1703.00014 [cond-mat.str-el].

[20] Y. Yoshida, S. Schröder, P. Ferriani, D. Serrate, A. Kubetzka, K. von Bergmann, S. Heinze, and R. Wiesendanger, "Conical Spin-Spiral State in an Ultrathin Film Driven by Higher-Order Spin Interactions," Phys. Rev. Lett. **108**, 087205 (2012).

[21] A. H. MacDonald, S. M. Girvin, and D. Yoshioka, "t/U expansion for the Hubbard model," Phys. Rev. B **37**, 9753 (1988).

[22] R. R. P. Singh, M. P. Gelfand, and D. A. Huse, "Ground States of Low-Dimensional Quantum Antiferromagnets," Phys. Rev. Lett. **61**, 2484 (1988).

[23] A. Chubukov, E. Gagliano, and C. Balseiro, "Phase diagram of the frustrated spin-1/2 Heisenberg antiferromagnet with cyclic-exchange interaction," Phys. Rev. B **45**, 7889 (1992).

[24] A. Läuchli, J. C. Domenge, C. Lhuillier, P. Sindzingre, and M. Troyer, "Two-Step Restoration of SU(2) Symmetry in a Frustrated Ring-Exchange Magnet," Phys. Rev. Lett. **95**, 137206 (2005), cond-mat/0412035.

[25] K. Majumdar, D. Furton, and G. S. Uhrig, "Effects of ring exchange interaction on the Néel phase of two-dimensional, spatially anisotropic, frustrated Heisenberg quantum antiferromagnet," Phys. Rev. B **85**, 144420 (2012), arXiv:1203.2598 [cond-mat.supr-con].

[26] S. Sachdev, M. A. Metlitski, Y. Qi, and C. Xu, "Fluctuating spin density waves in metals," Phys. Rev. B **80**, 155129 (2009), arXiv:0907.3732 [cond-mat.str-el].

[27] D. Chowdhury and S. Sachdev, "Higgs criticality in a two-dimensional metal," Phys. Rev. B **91**, 115123 (2015), arXiv:1412.1086 [cond-mat.str-el].

[28] N. Read and S. Sachdev, "Large N expansion for frustrated quantum antiferromagnets," Phys. Rev. Lett. **66**, 1773 (1991).

[29] X. G. Wen, "Mean-field theory of spin-liquid states with finite energy gap and topological orders," Phys. Rev. B **44**, 2664 (1991).

[30] F. A. Bais, P. van Driel, and M. de Wild Propitius, "Quantum symmetries in discrete gauge theories," Phys. Lett. B **280**, 63 (1992).

[31] J. M. Maldacena, G. W. Moore, and N. Seiberg, "D-brane charges in five-brane backgrounds," JHEP **10**, 005 (2001), arXiv:hep-th/0108152 [hep-th].

[32] T. H. Hansson, V. Oganesyan, and S. L. Sondhi, "Superconductors are topologically ordered," Annals of Physics **313**, 497 (2004), arXiv:cond-mat/0404327 [cond-mat.supr-con].

[33] R. K. Kaul, Y. B. Kim, S. Sachdev, and T. Senthil, "Algebraic charge liquids," Nature Physics **4**, 28 (2008), arXiv:0706.2187 [cond-mat.str-el].

[34] M. A. Metlitski, D. F. Mross, S. Sachdev, and T. Senthil, "Cooper pairing in non-fermi liquids," Phys. Rev. B **91**, 115111 (2015), arXiv:1403.3694 [cond-mat.str-el].

[35] M. E. Simon and C. M. Varma, "Detection and Implications of a Time-Reversal Breaking State in Underdoped Cuprates," Phys. Rev. Lett. **89**, 247003 (2002), cond-mat/0201036.

[36] S. Sachdev and R. Jalabert, "Effective lattice models for two dimensional quantum antiferromagnets," Mod. Phys. Lett. B **04**, 1043 (1990).

[37] F. D. M. Haldane, "O(3) Nonlinear σ Model and the Topological Distinction between Integer- and Half-Integer-Spin Antiferromagnets in Two Dimensions," Phys. Rev. Lett. **61**, 1029 (1988).

[38] N. Read and S. Sachdev, "Valence-bond and spin-Peierls ground states of low-dimensional quantum antiferromagnets," Phys. Rev. Lett. **62**, 1694 (1989).

[39] N. Read and S. Sachdev, "Spin-Peierls, valence-bond solid, and Néel ground states of low-dimensional quantum antiferromagnets," Phys. Rev. B **42**, 4568 (1990).

[40] T. Senthil, A. Vishwanath, L. Balents, S. Sachdev, and M. P. A. Fisher, "Deconfined Quantum Critical Points," Science **303**, 1490 (2004), cond-mat/0311326.

[41] E. Fradkin and S. H. Shenker, "Phase diagrams of lattice gauge theories with Higgs fields," Phys. Rev. D **19**, 3682 (1979).

[42] X. Yang and F. Wang, "Schwinger boson spin-liquid states on square lattice," Phys. Rev. B **94**, 035160 (2016), arXiv:1507.07621 [cond-mat.str-el].

[43] S. Chatterjee, Y. Qi, S. Sachdev, and J. Steinberg, "Superconductivity from a confinement transition out of a fractionalized Fermi liquid with Z_2 topological and Ising-nematic orders," Phys. Rev. B **94**, 024502 (2016), arXiv:1603.03041 [cond-mat.str-el].

[44] S. Sachdev, *Quantum Phase Transitions*, 2nd ed. (Cambridge University Press, Cambridge, UK, 2011).

[45] M. Inui and P. B. Littlewood, "Hartree-Fock study of the magnetism in the single-band Hubbard model," Phys. Rev. B **44**, 4415 (1991).

[46] E. Arrigoni and G. C. Strinati, "Doping-induced incommensurate antiferromagnetism in a Mott-Hubbard insulator," Phys. Rev. B **44**, 7455 (1991).

[47] M. Dzierzawa, "Hartree-Fock theory of spiral magnetic order in the 2-d Hubbard model," Z. Phys. B Cond. Mat. **86**, 49 (1992).

[48] P. A. Igoshev, M. A. Timirgazin, A. A. Katanin, A. K. Arzhnikov, and V. Y. Irkhin, "Incommensurate magnetic order and phase separation in the two-dimensional Hubbard model with nearest- and next-nearest-neighbor hopping," Phys. Rev. B **81**, 094407 (2010), arXiv:0912.0992 [cond-mat.str-el].

[49] J. G. Storey, "Hall effect and Fermi surface reconstruction via electron pockets in the high-T_c cuprates," Europhys. Lett. **113**, 27003 (2016), arXiv:1512.03112 [cond-mat.supr-con].

[50] A. Eberlein, W. Metzner, S. Sachdev, and H. Yamase, "Fermi Surface Reconstruction and Drop in the Hall Number due to Spiral Antiferromagnetism in High-T_c Cuprates," Phys. Rev. Lett. **117**, 187001 (2016), arXiv:1607.06087 [cond-mat.str-el].

[51] S. Chatterjee, S. Sachdev, and A. Eberlein, "Thermal and electrical transport in metals and superconductors across antiferromagnetic and topological quantum transitions," Phys. Rev. B **96**, 075103 (2017), arXiv:1704.02329 [cond-mat.str-el].

[52] M. Charlebois, S. Verret, A. Foley, O. Simard, D. Sénéchal, and A. Tremblay, "Hall effect in cuprates with incommensurate spin-density wave," (2017), arXiv:1708.09465 [cond-mat.str-el].

[53] M. S. Scheurer, S. Chatterjee, M. Ferrero, A. Georges, S. Sachdev, and W. Wu, unpublished (2017).